One-way optical modal transition based on causality in momentum space

Sunkyu Yu,[1] Xianji Piao,[1] KyungWan Yoo,[1] Jonghwa Shin,[2] and Namkyoo Park[1,*]

[1]*Photonic Systems Laboratory, School of EECS, Seoul National University, Seoul 151-744, South Korea*
[2]*Department of Materials Science and Engineering, KAIST, Daejeon 305–701, South Korea*
[*]*nkpark@snu.ac.kr*

Abstract: The concept of parity-time (PT) symmetry has been used to identify a route toward unidirectional dynamics in optical *k*-space: imposing asymmetry on the flow of light. Although PT-symmetric potentials have been implemented under the requirement of $V(x) = V^*(-x)$, this precondition has only been interpreted within the mathematical framework for the symmetry of Hamiltonians and has not been directly linked to unidirectionality induced by PT symmetry. In this paper, within the context of light-matter interactions, we develop an alternative route toward unidirectionality in *k*-space by employing the concept of causality. We demonstrate that potentials with real and causal momentum spectra produce unidirectional transitions of optical modes inside the *k*-continuum, which corresponds to an exceptional point on the degree of PT symmetry. Our analysis reveals a critical link between non-Hermitian problems and spectral theory and also enables multi-dimensional designer manipulation of optical modes, in contrast to the one-dimensional approach that used a Schrödinger-like equation in previous PT-symmetric optics.

OCIS codes: (080.6755) Systems with special symmetry; (070.7345) Wave propagation; (160.1190) Anisotropic optical materials; (050.5082) Phase space in wave optics.

References and links

1. M. Moharam and T. Gaylord, "Rigorous coupled-wave analysis of planar-grating diffraction," J. Opt. Soc. Am. **71**(7), 811–818 (1981).
2. J. A. Schuller, E. S. Barnard, W. Cai, Y. C. Jun, J. S. White, and M. L. Brongersma, "Plasmonics for extreme light concentration and manipulation," Nat. Mater. **9**(3), 193–204 (2010).
3. Z. Liu, H. Lee, Y. Xiong, C. Sun, and X. Zhang, "Far-field optical hyperlens magnifying sub-diffraction-limited objects," Science **315**(5819), 1686 (2007).
4. I. I. Smolyaninov, Y. J. Hung, and C. C. Davis, "Magnifying superlens in the visible frequency range," Science **315**(5819), 1699–1701 (2007).
5. X. Yang, J. Yao, J. Rho, X. Yin, and X. Zhang, "Experimental realization of three-dimensional indefinite cavities at the nanoscale with anomalous scaling laws," Nat. Photonics **6**(7), 450–454 (2012).
6. T. Pertsch, P. Dannberg, W. Elflein, A. Bräuer, and F. Lederer, "Optical Bloch oscillations in temperature tuned waveguide arrays," Phys. Rev. Lett. **83**(23), 4752–4755 (1999).
7. A. Block, C. Etrich, T. Limboeck, F. Bleckmann, E. Soergel, C. Rockstuhl, and S. Linden, "Bloch oscillations in plasmonic waveguide arrays," Nat. Commun. **5**, 3843 (2014).
8. K. Chung, S. Yu, C. J. Heo, J. W. Shim, S. M. Yang, M. G. Han, H. S. Lee, Y. Jin, S. Y. Lee, N. Park, and J. H. Shin, "Flexible, angle-independent, structural color reflectors inspired by Morpho butterfly wings," Adv. Mater. **24**(18), 2375–2379 (2012).
9. S. Yu, X. Piao, S. Koo, J. H. Shin, S. H. Lee, B. Min, and N. Park, "Mode junction photonics with a symmetry-breaking arrangement of mode-orthogonal heterostructures," Opt. Express **19**(25), 25500–25511 (2011).
10. C. M. Bender and S. Boettcher, "Real spectra in non-Hermitian hamiltonians having PT symmetry," Phys. Rev. Lett. **80**(24), 5243–5246 (1998).
11. C. M. Bender, D. C. Brody, and H. F. Jones, "Complex extension of quantum mechanics," Phys. Rev. Lett. **89**(27), 270401 (2002).
12. X. Zhu, H. Ramezani, C. Shi, J. Zhu, and X. Zhang, "PT-symmetric acoustics," Phys. Rev. X **4**(3), 031042 (2014).
13. L. Feng, M. Ayache, J. Huang, Y. L. Xu, M. H. Lu, Y. F. Chen, Y. Fainman, and A. Scherer, "Nonreciprocal light propagation in a silicon photonic circuit," Science **333**(6043), 729–733 (2011).

#243726 Received 25 Jun 2015; revised 14 Aug 2015; accepted 16 Aug 2015; published 15 Sep 2015

14. L. Feng, Y. L. Xu, W. S. Fegadolli, M. H. Lu, J. E. Oliveira, V. R. Almeida, Y. F. Chen, and A. Scherer, "Experimental demonstration of a unidirectional reflectionless parity-time metamaterial at optical frequencies," Nat. Mater. **12**(2), 108–113 (2012).
15. S. Fan, R. Baets, A. Petrov, Z. Yu, J. D. Joannopoulos, W. Freude, A. Melloni, M. Popović, M. Vanwolleghem, D. Jalas, M. Eich, M. Krause, H. Renner, E. Brinkmeyer, and C. R. Doerr, "Comment on "Nonreciprocal light propagation in a silicon photonic circuit," Science **335**(6064), 38, author reply 38 (2012).
16. D. Jalas, A. Petrov, M. Eich, W. Freude, S. Fan, Z. Yu, R. Baets, M. Popovic, A. Melloni, J. D. Joannopoulos, M. Vanwolleghem, C. R. Doerr, and H. Renner, "What is—and what is not—an optical isolator," Nat. Photonics **7**(8), 579–582 (2013).
17. K. G. Makris, R. El-Ganainy, D. N. Christodoulides, and Z. H. Musslimani, "Beam dynamics in PT symmetric optical lattices," Phys. Rev. Lett. **100**(10), 103904 (2008).
18. A. Guo, G. J. Salamo, D. Duchesne, R. Morandotti, M. Volatier-Ravat, V. Aimez, G. A. Siviloglou, and D. N. Christodoulides, "Observation of PT-symmetry breaking in complex optical potentials," Phys. Rev. Lett. **103**(9), 093902 (2009).
19. C. E. Rüter, K. G. Makris, R. El-Ganainy, D. N. Christodoulides, M. Segev, and D. Kip, "Observation of parity–time symmetry in optics," Nat. Photonics **6**, 192 (2010).
20. S. Yu, X. Piao, D. R. Mason, S. In, and N. Park, "Spatiospectral separation of exceptional points in PT-symmetric optical potentials," Phys. Rev. A **86**(3), 031802 (2012).
21. S. Yu, D. R. Mason, X. Piao, and N. Park, "Phase-dependent reversible nonreciprocity in complex metamolecules," Phys. Rev. B **87**(12), 125143 (2013).
22. S. Savoia, G. Castaldi, V. Galdi, A. Alù, and N. Engheta, "Tunneling of obliquely incident waves through PT-symmetric epsilon-near-zero bilayers," Phys. Rev. B **89**(8), 085105 (2014).
23. J. Xu, X. Zhuang, P. Guo, W. Huang, W. Hu, Q. Zhang, Q. Wan, X. Zhu, Z. Yang, L. Tong, X. Duan, and A. Pan, "Asymmetric light propagation in composition-graded semiconductor nanowires," Sci. Rep. **2**, 820 (2012).
24. S. Yu, H. S. Park, X. Piao, B. Min, and N. Park, "Low-dimensional optical chirality in complex potentials," arXiv:1409.0180 (2014).
25. S. Longhi, "PT-symmetric laser absorber," Phys. Rev. A **82**(3), 031801 (2010).
26. A. Regensburger, C. Bersch, M. A. Miri, G. Onishchukov, D. N. Christodoulides, and U. Peschel, "Parity-time synthetic photonic lattices," Nature **488**(7410), 167–171 (2012).
27. X. Zhu, L. Feng, P. Zhang, X. Yin, and X. Zhang, "One-way invisible cloak using parity-time symmetric transformation optics," Opt. Lett. **38**(15), 2821–2824 (2013).
28. B. Peng, Ş. K. Özdemir, S. Rotter, H. Yilmaz, M. Liertzer, F. Monifi, C. M. Bender, F. Nori, and L. Yang, "Loss-induced suppression and revival of lasing," Science **346**(6207), 328–332 (2014).
29. B. Peng, Ş. K. Özdemir, F. Lei, F. Monifi, M. Gianfreda, G. L. Long, S. Fan, F. Nori, C. M. Bender, and L. Yang, "Parity–time-symmetric whispering-gallery microcavities," Nat. Phys. **10**(5), 394–398 (2014).
30. L. Feng, Z. J. Wong, R. M. Ma, Y. Wang, and X. Zhang, "Single-mode laser by parity-time symmetry breaking," Science **346**(6212), 972–975 (2014).
31. L. Chang, X. Jiang, S. Hua, C. Yang, J. Wen, L. Jiang, G. Li, G. Wang, and M. Xiao, "Parity–time symmetry and variable optical isolation in active–passive-coupled microresonators," Nat. Photonics **8**(7), 524–529 (2014).
32. H. Hodaei, M. A. Miri, M. Heinrich, D. N. Christodoulides, and M. Khajavikhan, "Parity-time-symmetric microring lasers," Science **346**(6212), 975–978 (2014).
33. C. M. Bender, M. Gianfreda, Ş. K. Özdemir, B. Peng, and L. Yang, "Twofold transition in PT-symmetric coupled oscillators," Phys. Rev. A **88**(6), 062111 (2013).
34. D. Bohm, *Causality and Chance in Modern Physics* (Routledge, 2004).
35. H. M. Nussenzveig, *Causality and Dispersion Relations* (Academic Press, 1972).
36. J. V. Lorenzo-Ginori, "An approach to the 2D hilbert transform for image processing applications," in *Image Analysis and Recognition (*Springer Berlin Heidelberg, 2007), pp. 157–165.
37. M. Unser, "Splines: A perfect fit for signal and image processing," IEEE Signal Process. Mag. **16**(6), 22–38 (1999).
38. J. M. M. Senovilla, "Super-energy tensors," Class. Quantum Gravity **17**(14), 2799–2841 (2000).
39. S. G. Johnson, P. Bienstman, M. A. Skorobogatiy, M. Ibanescu, E. Lidorikis, and J. D. Joannopoulos, "Adiabatic theorem and continuous coupled-mode theory for efficient taper transitions in photonic crystals," Phys. Rev. E Stat. Nonlin. Soft Matter Phys. **66**(6), 066608 (2002).
40. G. Castaldi, S. Savoia, V. Galdi, A. Alù, and N. Engheta, "Analytical study of subwavelength imaging by uniaxial epsilon-near-zero metamaterial slabs," Phys. Rev. B **86**(11), 115123 (2012).
41. S. L. Hahn, "Multidimensional complex signals with single-orthant spectra," Proc. IEEE **80**(8), 1287–1300 (1992).
42. T. Bülow and G. Sommer, "Hypercomplex signals-A novel extension of the analytic signal to the multidimensional case," IEEE Trans. Signal Process. **49**(11), 2844–2852 (2001).
43. N. Bender, H. Ramezani, and T. Kottos, "Engineering wavefront caustics trajectories in PT-symmetric lattices," Opt. Lett. **40**(9), 2138–2141 (2015).
44. G. Q. Liang and Y. D. Chong, "Optical resonator analog of a two-dimensional topological insulator," Phys. Rev. Lett. **110**(20), 203904 (2013).
45. R. Fleury, D. L. Sounas, and A. Alù, "Negative refraction and planar focusing based on parity-time symmetric metasurfaces," Phys. Rev. Lett. **113**(2), 023903 (2014).
46. A. Mostafazadeh, "Pseudo-supersymmetric quantum mechanics and isospectral pseudo-Hermitian Hamiltonians," Nucl. Phys. B **640**(3), 419–434 (2002).

#243726 Received 25 Jun 2015; revised 14 Aug 2015; accepted 16 Aug 2015; published 15 Sep 2015

47. M. A. Miri, M. Heinrich, and D. N. Christodoulides, "Supersymmetry-generated complex optical potentials with real spectra," Phys. Rev. A **87**(4), 043819 (2013).

1. Introduction

Optical modes are one of the critical features for defining the flow of light, by determining the 'momentum' (or wavevector k) of photons for a given spatial distribution of optical potentials. In the context of light-matter interactions, the manipulation of optical modes and wavevectors through the modulation of refractive index landscapes (or optical potentials) is not only a classical subject, as observed in a diffraction grating [1], but is also an emerging area of research involved in recent discoveries in the field of optics, e.g., subwavelength plasmonics [2] and indefinite metamaterials [3–5] with high-k components, optical Bloch oscillations [6,7] based on a graded-k design, bio-mimic reflective surface [8] with randomly-distributed k, and drastic optical manipulation using modal orthogonality [9]. Although extremely encouraging, all of these achievements were obtained by controlling only the real-valued optical potentials within the well-known restriction of Hermiticity in quantum mechanics and optics for real eigenvalues. Because real potentials correspond only to double-sided spectra in Fourier space, the considerable opportunities afforded by complex potentials of generalized spectra have been overlooked.

From a mathematical perspective, continuous efforts have been focused on overcoming the Hermitian restriction for real eigenvalues. Bender first proved the existence of real eigenvalues for complex potentials [10] when the potentials satisfy parity-time (PT) symmetry. This striking discovery has been adopted in various fields [11,12] to interpret the physics of complex potentials. In the field of optics, although Lorentz reciprocity cannot be broken with only spatially varying complex potentials [13–16], the use of cleverly designed PT-symmetric potentials has resulted in inspiring achievements, such as in the unidirectional coupling dynamics of linear [17–23] and angular [24] optical momenta, a simultaneously operated laser and perfect absorber [25], unidirectional invisibility from asymmetric reflection [26,27], and spectral realizations of PT-symmetry exploiting optical resonances [28–33]. Because PT-symmetric optics were initially developed as an effective model of quantum-mechanical problems, optical potentials in subsequent PT-symmetric applications have been designed to simply fulfill the condition of $V(x) = V^*(-x)$, which is derived from the commutative relation between PT and the Hamiltonian operators for a Schrödinger-like equation. Interestingly, however, investigations of the PT-symmetric potential $V(x)$ in the Fourier domain, which has the intriguing consequence that the potential momentum of $F\{V(x)\}$ is real-valued, for example, have not been attempted. Because the directional shift in momentum space is the underlying physics of PT-symmetric optical phenomena [13–24,26,27], a more thorough investigation of the potential momentum $F\{V(x)\}$ will provide new insight into PT-symmetric optics in terms of momentum interactions between light and potentials.

In this paper, we propose a novel pathway toward unidirectional coupling in k-space in the context of light-matter momentum interactions to demonstrate the role of potential momentum $F\{V(x)\}$. We start from the general problem of light excursions in k-space, focusing on 'unidirectional modal transitions' along the isofrequency contour (IFC). Under the weak-coupling regime, we then demonstrate that 'causality' in potential momentum space, *i.e.,* causal potential momentum, produces a unidirectional k-transition of light inside the IFC k-continuum, corresponding to exceptional point (EP) dynamics on the degree of PT symmetry. Our results provide a logical mechanism for understanding PT symmetry through spectral analysis and enable the 'design' of momentum shifts through potential modulations rather than the 'observation' of momentum shifts at given PT-symmetric potentials, thereby providing designers control of optical modes, such as for collimated beam steering or excitations in the extreme regime of low- or high-k states.

Figure 1 shows examples of light excursions in k-space. Because the wavevector k affects the direction and effective wavelength of wave propagation, applications such as beam steering (controlling the direction, Figs. 1(a) and 1(b)) and high- / low-k excitation

#243726 Received 25 Jun 2015; revised 14 Aug 2015; accepted 16 Aug 2015; published 15 Sep 2015

(controlling the wavelength, Fig. 1(c) and Fig. 1(d), respectively) could be enabled through modification of wavevectors. To tailor the evolution of the optical state in *k*-space, we address the unidirectionality for the modal transition along the IFC (red arrows in Fig. 1), which suppresses the back transfer (gray arrows in Fig. 1) to the initial state, thereby efficiently delivering optical energy into the targeted mode. It is noted that the unidirectional modal transition can be understood in the context of the relation between 'cause' (the initial state with incident waves) and 'effects' (the directionally excited states from the unidirectional coupling) along the IFC (Fig. 1(e)). This description naturally leads to the concept of 'causality' [34,35], which has usually been used to define the relation between an event and the following results in the temporal domain, *e.g.* Kramers-Kronig relation [35]. We note that the genenalized concept of causality has not restricted to the temporal domain [35] but widely extended to various physical axes, including spectral [36], spatial [37] or momentum [38] domains. In the following discussions we employ the notion of causality in the *k*-axis [38] (red arrows in Fig. 1(e)) rather than the time axis, *i.e.* causal momentum, as analugous to non-temporal applications [36–38].

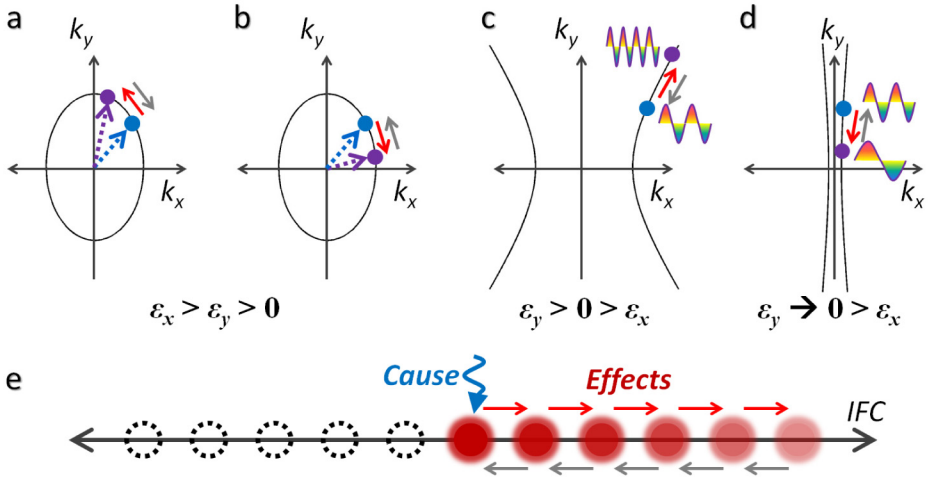

Fig. 1. Schematics of one-way transitions along (a, b) elliptic, (c) hyperbolic, and (d) quasi-linear IFCs. (a) Counterclockwise and (b) clockwise transitions; dotted lines denote the direction of the flow of light for beam steering. (c) High-*k* and (d) low-*k* excitations. Blue (or purple) circles denote the initial (or excited) state for each IFC. (e) Schematic linking one-way optical transition with causality. Red (or gray) arrows show allowed (or forbidden) transitions along the IFC in (a-e).

2. Coupled mode equation in 2-dimensional anisotropic materials

To investigate the relationship between one-way transitions and causality, by generalizing the continuous coupled mode theory [39] to 2-dimensional anisotropic materials, we derive the coupled mode equation for analyzing the coupling and energy transfer between optical modes. Without loss of generality, we consider a TM-polarized wave in a nonmagnetic anisotropic material (H_z, E_x, and E_y with $\varepsilon_{x,y}$) that produces a *k*-continuum for an elliptic IFC (Figs. 1(a) and 1(b)), a hyperbolic IFC [3–5] (Fig. 1(c)), or a quasi-linear IFC with extreme anisotropy [40] (Fig. 1(d)) in *k*-space. Here, we apply two standard approximations to the time-harmonic wave equation at a frequency ω: a weak ($|\Delta\varepsilon_{x,y}(x,y)| << |\varepsilon_{x0,y0}|$, where $\varepsilon_{x,y}(x,y) = \varepsilon_{x0,y0} + \Delta\varepsilon_{x,y}(x,y)$) and a slowly-varying modulated potential ($|\Delta\varepsilon_y^{-1}\cdot\partial_x\Delta\varepsilon_y| << |k_x|$ and $|\Delta\varepsilon_x^{-1}\cdot\partial_y\Delta\varepsilon_x| << |k_y|$). We use the IFC relation of $k_0^2 = k_x^2/\varepsilon_{y0} + k_y^2/\varepsilon_{x0}$, where $k_0 = \omega/c$ is the free-space wavenumber, to derive the following expression (see Appendix A)

$$\iint(\vec{\beta}_{\vec{k}}\cdot\vec{\sigma}_{\vec{k}}(x,y))\psi_{[k_x,k_y]}e^{-i(k_x x+k_y y)}dk_x dk_y = 2i\cdot\iint\nabla\cdot(\vec{\beta}_{\vec{k}}\psi_{[k_x,k_y]})e^{-i(k_x x+k_y y)}dk_x dk_y, \quad (1)$$

#243726 Received 25 Jun 2015; revised 14 Aug 2015; accepted 16 Aug 2015; published 15 Sep 2015

where $\psi_{[kx,ky]}$ is the spatially varying envelope [39] of the magnetic field imposed on the planewave solution $exp(-ik_x{\cdot}x\text{-}ik_y{\cdot}y)$ as $H_z(x,y) = \iint\psi_{[kx,ky]}(x,y){\cdot}exp(-ik_x{\cdot}x\text{-}ik_y{\cdot}y)dk_xdk_y$, $\boldsymbol{\beta_k} = (k_x{\cdot}\varepsilon_{y0}^{-1})\boldsymbol{x} + (k_y{\cdot}\varepsilon_{x0}^{-1})\boldsymbol{y}$ is the ε-normalized wavevector, and $\boldsymbol{\sigma_k}(x,y) = (k_x{\cdot}\Delta\varepsilon_y(x,y)/\varepsilon_{y0})\boldsymbol{x} + (k_y{\cdot}\Delta\varepsilon_x(x,y)/\varepsilon_{x0})\boldsymbol{y}$ is the local modulation vector. Equation (1) clearly shows the source of the modal transitions $\boldsymbol{\beta_k}{\cdot}\boldsymbol{\sigma_k}(x,y)$ that induce the locally modulated envelope $\nabla\psi$. Additionally, note that $\psi_{[kx,ky]}$ corresponds to the amplitude of the k-space optical mode $\boldsymbol{k} = (k_x,k_y)$.

With the Fourier expansion ($\Delta\varepsilon_{pq}(p,q)$) of the modulated potential $\Delta\varepsilon(x,y)$ and the use of the divergence theorem, the 2-dimensional coupled mode equation between the optical modes of $\boldsymbol{k} = (k_x,k_y)$ and $(k_{x\text{-}p},k_{y\text{-}q})$ is now obtained as

$$\begin{aligned} &8\pi^2 i\cdot\oint_S \psi_{[k_x,k_y]}\vec{\beta}_{\vec{k}}\cdot d\vec{s} \\ &= \int_V\iiint_{-\infty}^{\infty}\left(\frac{(k_x-p)^2\Delta\varepsilon_{ypq}}{\varepsilon_{y0}^2}+\frac{(k_y-q)^2\Delta\varepsilon_{xpq}}{\varepsilon_{x0}^2}\right)\psi_{[k_x-p,k_y-q]}dpdqdv. \end{aligned} \tag{2}$$

3. Design of one-way coupling potentials

Equation (2) defines the coupling along the IFC $k_0^2 = k_x^2/\varepsilon_{y0} + k_y^2/\varepsilon_{x0}$ (including the multipath coupling through $\Delta\varepsilon_{pq}(p,q)$ with a finite bandwidth) and can be used to derive the criterion for the directional coupling that prohibits back transfers (gray arrows in Fig. 1). Note that the potential momentum $\Delta\varepsilon_{pq}$ in Eq. (2) mediates the coupling between states, and a highly efficient unidirectional modal transition can be obtained by enforcing a restriction in potential momentum space (p,q), such as $\Delta\varepsilon_{pq} \neq 0$ only for a single quadrant, to achieve a zero value for the integral of the back transfer. Such a restriction can indeed be realized with the causality condition in multi-dimensions by replacing the axis condition $k > 0$ with the quadrant condition $k_x > 0$ and $k_y > 0$, defined by the multi-dimensional Hilbert transform for single orthant spectra [41,42]. The selection of a nonzero quadrant is also clearly determined by the transition direction, e.g., the high-k excitation toward larger k (the red arrow in Fig. 1(c)) is produced by restricting the potential momentum to the 1st quadrant ($p,q \geq 0$), whereas the low-k excitation toward smaller k (red arrow in Fig. 1(d)) is produced by selecting the 3rd quadrant spectrum ($p,q \leq 0$).

The implementation of the aforementioned conditions in the momentum and spatial domains can easily be achieved by employing the multi-dimensional Hilbert transform for single orthant spectra [41,42], such as $\Delta\varepsilon_{pq} = [1 \pm sgn(p) \pm sgn(q) + sgn(p){\cdot}sgn(q)]{\cdot}\Delta\varepsilon_{rpq}(p,q)/4$, where the upper (lower) sign refers to the high- (low-) k excitation, $\Delta\varepsilon_{rpq}^*(-p,-q) = \Delta\varepsilon_{rpq}(p,q)$, where $\Delta\varepsilon_r(x,y) = (1/4\pi^2)\cdot\iint\Delta\varepsilon_{rpq}(p,q)\cdot exp(-ipx\text{-}iqy)dpdq$ is a real function. In the spatial domain, the "unidirectional coupling potentials" for the low-k and high-k excitations then become

$$\begin{aligned} &\Delta\varepsilon_{L,H}(x,y) \\ &= \frac{1}{4}\left(\Delta\varepsilon_r(x,y) - \frac{1}{\pi^2}\int_{-\infty}^{\infty}\int_{-\infty}^{\infty}\frac{\Delta\varepsilon_r(x',y')}{(x-x')(y-y')}dx'dy'\right), \\ &\pm\frac{i}{4\pi}\left(\int_{-\infty}^{\infty}\frac{\Delta\varepsilon_r(x',y)}{x-x'}dx' + \int_{-\infty}^{\infty}\frac{\Delta\varepsilon_r(x,y')}{y-y'}dy'\right) \end{aligned} \tag{3}$$

or simply $\Delta\varepsilon_{L,H} = \{[\Delta\varepsilon_r - H_T(\Delta\varepsilon_r)] \pm i[H_{px}(\Delta\varepsilon_r) + H_{py}(\Delta\varepsilon_r)]\}/4$, where $\Delta\varepsilon_L$ ($\Delta\varepsilon_H$) is the potential for the low- (or high-) k excitation with the upper (or lower) sign, and H_T (or H_p) is the total (or partial) Hilbert transform [41,42]. We emphasize that Eq. (3) not only reveals that complex potentials in the spatial domain are essential for producing unidirectional modal transitions but also that the PT-symmetric complex potentials of $\Delta\varepsilon_0{\cdot}exp(-ip_0x)$ that have been previously studied [13,14,23] are only a manifestation of a special case, i.e., pointwise unidirectional coupling ($\Delta\varepsilon_{rp} = \Delta\varepsilon_0{\cdot}\pi[\delta(p-p_0) + \delta(p + p_0)]$) in a 1-dimensional problem. Note

#243726 Received 25 Jun 2015; revised 14 Aug 2015; accepted 16 Aug 2015; published 15 Sep 2015

that our formalism based on potential momentum causality allows the deterministic design of potentials for unidirectional modal transitions: from the $\Delta\varepsilon_{rpq}$ in potential momentum space. This condition can easily be extended to isofrequency 'surfaces' in 3-dimensional problems by employing a 3-dimensional Hilbert transform [41,42].

4. Link between PT symmetry and causality in potential momentum space

Most importantly, Eq. (3) offers implicit link between PT symmetry [10–33] and causality in potential momentum space, which, to the best of our knowledge, has not been previously elucidated. The unidirectional coupling potentials of Eq. (3) from causality satisfy the necessary condition [10] for PT symmetry $\Delta\varepsilon_{L,H}(x,y) = \Delta\varepsilon_{L,H}^*(-x,-y)$ and also guarantee real-valued spectra in momentum space (p,q). Because 'perfect' modal unidirectionality in PT-symmetric potentials is achieved only at the EP [17–22,24] where PT symmetry breaking occurs, we note that the causality potentials of Eq. (3) that have unidirectionality correspond to the EP on the degree of PT symmetry (within the approximations of weak and slowly varying modulation; see Appendix A). Accordingly, the regimes before and after the EP will correspond to noncausal, real-valued spectra in potential momentum space.

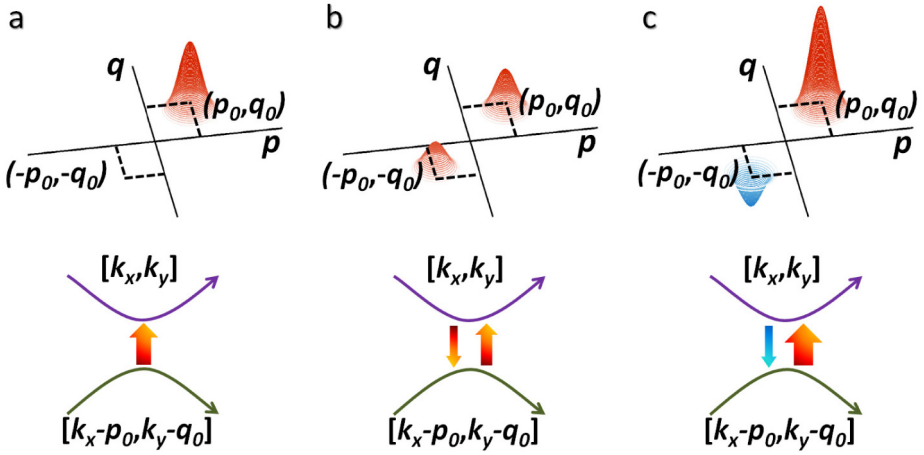

Fig. 2. Potential momentum spectra for degrees of PT symmetry: (a) at the EP ($\Delta\varepsilon_{sr0} = \Delta\varepsilon_{si0}$), (b) before the EP ($\Delta\varepsilon_{sr0} > \Delta\varepsilon_{si0}$), and (c) after the EP ($\Delta\varepsilon_{sr0} < \Delta\varepsilon_{si0}$). Lower figures illustrate the corresponding coupling between momentum states for each degree. Green (purple) solid line denotes the momentum state that corresponds to the 'cause' ('effect'). As shown, causality is only maintained at the EP. Gaussian spectra with $\sigma = 0.25$ and $p_0 = q_0 = 1$ are assumed, without loss of generality.

We illustrate the aforementioned results with a PT-symmetric potential $\Delta\varepsilon_s(x,y)$ in space, where $Re[\Delta\varepsilon_s]$ (or $Im[\Delta\varepsilon_s]$) is an even (or odd) real-valued function that satisfies the precondition $\Delta\varepsilon_s(x,y) = \Delta\varepsilon_s^*(-x,-y)$. The potential momentum $\Delta\varepsilon_m(p,q) = F\{\Delta\varepsilon_s(x,y)\}$ is then expressed by the sum of real-valued functions as $\Delta\varepsilon_m(p,q) = \Delta\varepsilon_{m\text{-}even}(p,q) + \Delta\varepsilon_{m\text{-}odd}(p,q)$, where $\Delta\varepsilon_{m\text{-}even} = F\{Re[\Delta\varepsilon_s(x,y)]\}$ is an even function and $\Delta\varepsilon_{m\text{-}odd} = -Im[F\{Im[\Delta\varepsilon_s(x,y)]\}]$ is an odd function. To clarify the relation between the degree of PT symmetry and the potential momentum, we assume the simplest potential for which the real and imaginary parts of $\Delta\varepsilon_s(x,y)$ with a Gaussian envelope $\Delta\varepsilon_s(x,y) = [\Delta\varepsilon_{sr0} \cdot cos(p_0x + q_0y) + i\Delta\varepsilon_{si0} \cdot sin(p_0x + q_0y)] \cdot exp(-(x^2 + y^2)/(2\sigma^2))$, where both $\Delta\varepsilon_{sr0}$ and $\Delta\varepsilon_{si0}$ are real values and $\Delta\varepsilon_{sr0} = \Delta\varepsilon_{si0}$ at the EP. Figure 2 shows the calculated potential momentum at each different degree of PT symmetry. Although the spectrum of the potential momentum satisfies causality ($p,q \geq 0$) at the EP (Fig. 2(a)), the potentials of the regimes before (Fig. 2(b)) and after (Fig. 2(c)) the EP break causality. In this respect, the concept of PT symmetry breaking can be interpreted as a phase transition from an in-phase potential momentum spectrum to an out-of-phase potential momentum spectrum (Fig. 2(b) vs. Fig. 2(c)) separated by the causal phase (Fig. 2(a)).

#243726 Received 25 Jun 2015; revised 14 Aug 2015; accepted 16 Aug 2015; published 15 Sep 2015

Note that the above interpretation provides an intuitive understanding of the degree of PT symmetry, providing a perspective not restricted to the relative magnitude between the real and imaginary parts of the potentials [17–22,24] but rather from a direct spectral analysis of the 'degree of the causality' for the real-valued potential momentum. Furthermore, with the multi-dimensional expression of Eq. (3), our results allow the multi-dimensional extension of the PT-symmetric condition to overcome the one-dimensional effective model [13–27] based on the paraxial wave equation in the description of PT-symmetric optics.

5. High-*k* excitations in indefinite materials

Without loss of generality, we investigate a case of high-k excitations along the hyperbolic IFC ($p,q \geq 0$, Fig. 1(c)). Although high-k features of hyperbolic metamaterials provide an ideal template for subwavelength imaging [3,4] or light confinement [5], the large mismatch in k-vector hinders the excitation of high-k modes in the indefinite IFC. Here, we apply the unidirectional modal transition for the adiabatic transfer of optical energy to the high-k state. A y-axis-invariant wave incident on a unidirectional potential ($x \geq 0$) from the left side ($k_{x0} > 0$) is considered, as illustrated in Fig. 3(a). Note that potentials of arbitrary shape can be accommodated by discretizing the potential in both the spatial (Fig. 3(a)) and momentum (Fig. 3(b)) domains. By setting the y-infinite unit volume V with a deep-subwavelength spatial discretization Δx, the surface integral of Eq. (2) is determined on the $S_L(x_L)$ and $S_R(x_R)$ surfaces, and the volume integral can be evaluated from the average of the values in S_L and S_R. The discretization for the momentum states was also performed on the IFC (circles in Fig. 3(b)) from the phase-matching condition. The discretized form of Eq. (2) is then expressed as

$$\int_{S_R} \psi_m(x_R, y)dy = \int_{S_L} \psi_m(x_L, y)dy + \sum_{n=1}^{m} \frac{\varepsilon_{y0}\Delta x \cdot \Delta p_n \Delta q_n}{16\pi^2 i k_{xm}} \cdot \left(\frac{k_{xn}^{\,2}\Delta\varepsilon_{ypq}}{\varepsilon_{y0}^2} + \frac{k_{yn}^{\,2}\Delta\varepsilon_{xpq}}{\varepsilon_{x0}^2} \right) \cdot \int_{S_L+S_R} \psi_n dy, \quad (4)$$

where the subscript m denotes the m-th momentum state of (k_{xm},k_{ym}); $n = 1$ is the incident state; $p = k_{xm} - k_{xn}$; $q = k_{ym} - k_{yn}$; $\Delta p_n = k_{x(n+1)} - k_{xn}$; and $\Delta q_n = k_{y(n+1)} - k_{yn}$. Equation (4) can be used to perform a serial numerical calculation for the integral of the envelope, starting from the left boundary (detailed procedure for the serial calculation is provided in the Appendix B). As a result of the causality condition that is imposed on $\Delta\varepsilon_{pq}$, only the eigenstates on the bounded region of the IFC (blue circles in Fig. 3(b)) participate in the coupling to the (k_x,k_y) state.

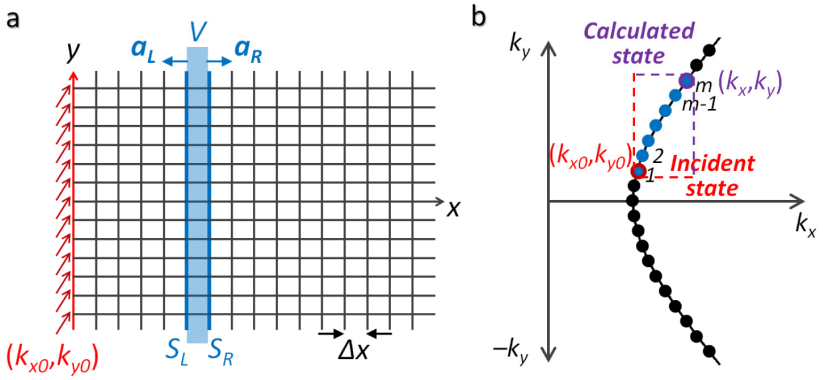

Fig. 3. Discretization of (a) spatial and (b) momentum domains for the derivation of Eq. (4). S_L and S_R present the left and right surfaces, respectively, of the unit volume V (in blue). A wave with a unit amplitude (at the (k_{x0},k_{y0}) state, shown by red arrows in (a)) is incident on the left side of the spatial domain. Circles in (b) represent discretization in momentum space. Blue circles denote states that participate in the coupling to the calculated state (k_x, k_y).

#243726 Received 25 Jun 2015; revised 14 Aug 2015; accepted 16 Aug 2015; published 15 Sep 2015

The high-k excitation process is shown in Fig. 4. For general curvilinear IFCs, the transition through the multiple linear-path coupling should be adopted, as shown in the example presented in Fig. 4(a). In this specific example, we assume a potential modulation that provides five real-valued momentum spectra (Fig. 4(b)) for multiple transitions. A finite bandwidth is used for each spectrum to accommodate quasi-phase matching. Figures 4(c) and 4(d) show the normalized amplitude and phase of the complex potential given by Eq. (3) and present the confinement in space from the finite bandwidth and the mixed phase evolution from the multi-harmonics. From Figs. 4(c) and 4(d), the spatial profiles of anisotropic permittivity are determined as $\varepsilon_x(x,y) = \varepsilon_{x0} + \Delta\varepsilon_x(x,y)$ and $\varepsilon_y(x,y) = \varepsilon_{y0} + \Delta\varepsilon_y(x,y)$. This spatially-varying *anisotropic* material can be realized with spatially-varying, one-dimensional alternating layers composed of *isotropic* materials, in the regime of the effective medium theory (EMT) [3–5]. To validate the use of EMT with practical material parameters, we restrict the maximum variation of ε_x and ε_y to 20%, and the spatial variation is slow enough compared to the wavelength (p / k_0 ~0.2 and q / k_0 < 0.8), enabling the realization based on metamaterial platforms.

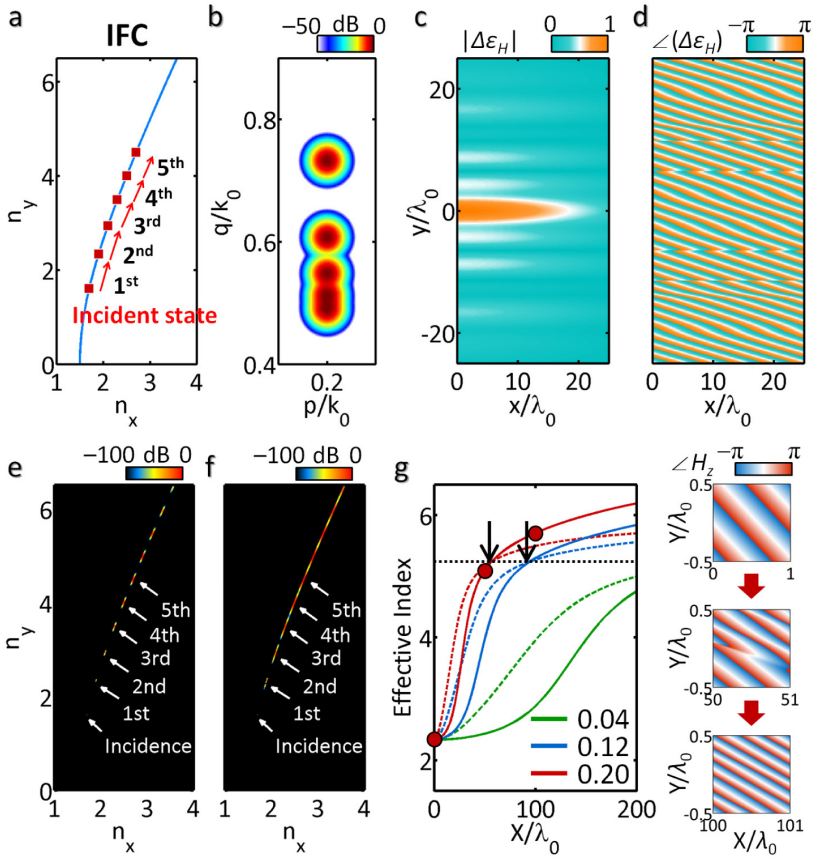

Fig. 4. High-k excitations along the hyperbolic IFC ($\varepsilon_{x0} = -9$, $\varepsilon_{y0} = 2.25$). (a) Design strategy with 5-stage transitions. (b) Normalized real-valued momentum spectra of $\Delta\varepsilon_{pq}$ (Gaussian bandwidth of $\sigma_{x,y} = k_0/100$ for each spectrum). (c) Normalized amplitude and (d) phase of the corresponding complex potential in the spatial domain. The profile of momentum spectra in (b) is assigned to both $\Delta\varepsilon_{xpq}$ and $\Delta\varepsilon_{ypq}$. The amplitude of the envelopes in momentum space at $x = 100\lambda_0$ are shown for different bandwidths of (e) $\sigma_{x,y} = k_0/200$ and (f) $\sigma_{x,y} = k_0/100$. (g) Variation in the effective index along the x-axis for different bandwidths (solid lines show $\sigma_{x,y} = k_0/100$, and dotted lines show $\sigma_{x,y} = k_0/200$). The phase of the magnetic field at each position (red circles in 4g) is also shown in the right panel of (g). Maximum values of modulations are $\Delta\varepsilon_x(x,y)/\varepsilon_{x0} = \Delta\varepsilon_y(x,y)/\varepsilon_{y0} = 0.04$, 0.12, and 0.20. Discretization parameters at the deep-subwavelength scale are $\Delta x = \lambda_0/50$, $\Delta k_y = k_0/100$, and $\Delta p = \Delta q = \sigma_{x,y}/10$ for all cases.

#243726 Received 25 Jun 2015; revised 14 Aug 2015; accepted 16 Aug 2015; published 15 Sep 2015

Figures 4(e) and 4(f) present the results for high-k excitations in k-space at the point $x = 100\lambda_0$ for different bandwidths of the potential momentum spectra. The variation in the effective index along the x-axis is illustrated in Fig. 4(g), using $n_{eff}(x) = \iint n(k_x,k_y)\cdot|\psi_{[kx,ky]}(x)|^2 dk_x dk_y \,/\, \iint|\psi_{[kx,ky]}(x)|^2 dk_x dk_y$ and the excited envelopes at each x value. For all cases, successful multistage delivery of optical energy to the high-k regime is observed and is found to be more efficient for larger modulation depths (Fig. 4(g)). Notably, even the higher-k states are excited above the targeted final (5th) state (black dotted line in Fig. 4(g)), which results from the linear asymptotic behavior of the hyperbolic IFC ($k_y \sim(-\varepsilon_x/\varepsilon_y)^{1/2}\cdot k_x$) that alleviates the phase-matching condition in the high-k regime. This result indicates that a perpetual transition to higher-k states becomes possible for the hyperbolic IFC, provided that the minor phase-mismatch is compensated by the bandwidth of the modulation spectra, as evidenced by the superior excitations in the high-k regime with the application of broadband potentials (solid vs. dotted lines after the arrows in Fig. 4(g)).

6. Collimated beam steering in definite materials

Figure 5 shows another application to definite materials, in which selective transitions are determined by the lateral component k_y of the wavevector. For clockwise beam steering along the elliptic IFC (Fig. 5(a), with the nonzero 4th quadrant of (p,q) space), the transition is allowed only within the 1st quadrant of the IFC, as can be clearly observed from the transition states (red squares) along the IFC. Figure 5(b) shows the beam trajectories in spatial domain calculated from Eq. (4) and confirms that strong, selective beam steering occurs only with lateral positive wavevector components k_{y0}, as predicted. In contrast to the high-k excitation example with asymptotic behavior (Figs. 4(e)-4(g)), we note that in this case, selective convergence toward the final k state is obtained, facilitating asymmetric steering and collimation of the beam (blue solid lines, angular bandwidth from 44° to 17°).

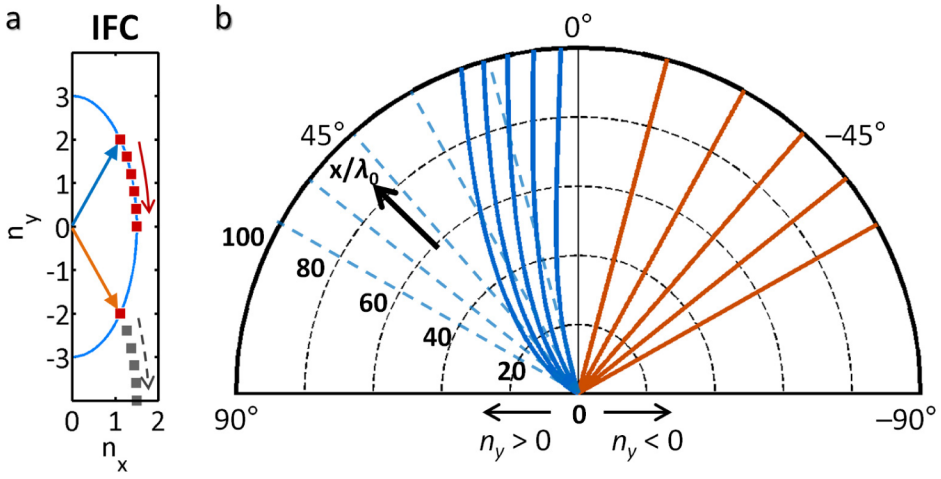

Fig. 5. Nonreciprocal beam steering and collimation in the elliptic IFC ($\varepsilon_{x0} = 9$, $\varepsilon_{y0} = 2.25$). (a) IFC with 5-stage transitions. Red (gray) squares denote allowed (forbidden) states for the transition. (b) Beam trajectories (solid lines) for different incidences of $n_y > 0$ (blue dotted lines) and $n_y < 0$ (orange). Maximum values of modulations are $\varepsilon_x(x,y)/\varepsilon_{x0} = \varepsilon_y(x,y)/\varepsilon_{y0} = 0.2$. $\sigma_{x,y} = k_0/200$. All other parameters of the potential are the same as those presented in Fig. 4.

7. Conclusion

Our approach offers a fundamental understanding of the degree of PT symmetry in terms of *causal momentum interactions* between light and potentials to allow the multi-dimensional extension of the PT-symmetric condition, and provides us with the ability to tailor optical evolution in k-space via *unidirectional* complex potentials directly designed in k-space. We have demonstrated novel applications, such as excitations in the extreme k regime and

#243726 Received 25 Jun 2015; revised 14 Aug 2015; accepted 16 Aug 2015; published 15 Sep 2015

nonreciprocal beam steering and collimation. Although we assumed the realization in continuous permittivity landscape in these applications, our analysis linking the causality in *k*-space and PT symmetry can be extended into more practical platforms such as photonic molecules composed of discrete optical elements (*e.g.* optical waveguides [21,43], resonators [44], or lumped RLC elements [45]), simply by applying discrete Fourier transform. A further application for complex potentials could also be made in the frequency ω domain, i.e., using time-varying complex potentials for temporal non-Hermitian dynamics. It is envisaged that the relation between causality and a *complex* potential momentum may also provide a clue to the physical interpretation of *non*-PT-symmetric potentials [46,47] with real spectra.

Appendix A: Detailed derivation of Eq. (1)

For spatially varying materials, the time-harmonic wave equation at a frequency ω takes the following form:

$$k_0^2 H_z = -\varepsilon_y^{-1}\partial_x^2 H_z - \varepsilon_x^{-1}\partial_y^2 H_z - \partial_x\varepsilon_y^{-1}\cdot\partial_x H_z - \partial_y\varepsilon_x^{-1}\cdot\partial_y H_z, \tag{5}$$

where $k_0 = \omega/c$ is the free-space wavenumber. Here, we apply two standard approximations of weakly and slowly varying modulated potentials to the time-harmonic wave equation. In the weak coupling regime ($|\Delta\varepsilon_{x,y}(x,y)| << |\varepsilon_{x0,y0}|$, where $\varepsilon_{x,y}(x,y) = \varepsilon_{x0,y0} + \Delta\varepsilon_{x,y}(x,y)$), the field can be expanded using a spatially varying envelope $\psi_{[kx,ky]}$ as follows: $H_z(x,y) = \iint\psi_{[kx,ky]}(x,y)\cdot exp(-ik_x\cdot x - ik_y\cdot y)dk_x dk_y$. Then, Eq. (5) becomes

$$\begin{aligned}&\iint\left[k_0^2 - \left(\frac{k_x^2}{\varepsilon_y} + \frac{k_y^2}{\varepsilon_x}\right) + i\left(k_x\partial_x\varepsilon_y^{-1} + k_y\partial_y\varepsilon_x^{-1}\right)\right]\psi_{[k_x,k_y]}e^{-i(k_x x + k_y y)}dk_x dk_y.\\ &= \iint 2i\cdot\left(\frac{k_x\partial_x\psi_{[k_x,k_y]}}{\varepsilon_y} + \frac{k_y\partial_y\psi_{[k_x,k_y]}}{\varepsilon_x}\right)e^{-i(k_x x + k_y y)}dk_x dk_y\end{aligned} \tag{6}$$

Assuming that the modulations are weak, i.e., $|\Delta\varepsilon_{x,y} / \varepsilon_{x0,y0}| << 1$, and the IFC relation $k_0^2 = k_x^2/\varepsilon_{y0} + k_y^2/\varepsilon_{x0}$, Eq. (6) can be approximated as follows:

$$\begin{aligned}&\iint\left[\frac{k_x\left(\Delta\varepsilon_y k_x - i\partial_x\Delta\varepsilon_y\right)}{{\varepsilon_{y0}}^2} + \frac{k_y\left(\Delta\varepsilon_x k_y - i\partial_y\Delta\varepsilon_x\right)}{{\varepsilon_{x0}}^2}\right]\psi_{[k_x,k_y]}e^{-i(k_x x + k_y y)}dk_x dk_y.\\ &\cong \iint 2i\cdot\left[\frac{k_x\partial_x\psi_{[k_x,k_y]}}{\varepsilon_{y0}} + \frac{k_y\partial_y\psi_{[k_x,k_y]}}{\varepsilon_{x0}}\right]e^{-i(k_x x + k_y y)}dk_x dk_y\end{aligned} \tag{7}$$

The left-hand side of Eq. (7) corresponds to the *source* of the spatially varying envelope $\partial\psi$ that appears on the right-hand side of the equation. Assuming that the modulations are slowly varying, i.e., ($|\Delta\varepsilon_y^{-1}\cdot\partial_x\Delta\varepsilon_y| << |k_x|$ and $|\Delta\varepsilon_x^{-1}\cdot\partial_y\Delta\varepsilon_x| << |k_y|$), the first-order derivatives of $\Delta\varepsilon_{x,y}$ can be neglected, and Eq. (7) becomes

$$\begin{aligned}&\iint\left[\frac{k_x}{\varepsilon_{y0}}\cdot\frac{\Delta\varepsilon_y}{\varepsilon_{y0}}k_x + \frac{k_y}{\varepsilon_{x0}}\cdot\frac{\Delta\varepsilon_x}{\varepsilon_{x0}}k_y\right]\psi_{[k_x,k_y]}e^{-i(k_x x + k_y y)}dk_x dk_y.\\ &\cong \iint 2i\cdot\left[\frac{k_x}{\varepsilon_{y0}}\cdot\partial_x\psi_{[k_x,k_y]} + \frac{k_y}{\varepsilon_{x0}}\cdot\partial_y\psi_{[k_x,k_y]}\right]e^{-i(k_x x + k_y y)}dk_x dk_y\end{aligned} \tag{8}$$

We simplify Eq. (8) by introducing the ε-normalized wavevector $\beta_k = (k_x\cdot\varepsilon_{y0}^{-1})x + (k_y\cdot\varepsilon_{x0}^{-1})y$ and the local modulation vector $\sigma_k(x, y) = (k_x\cdot\Delta\varepsilon_y(x, y)/\varepsilon_{y0})x + (k_y\cdot\Delta\varepsilon_x(x, y)/\varepsilon_{x0})y$, which results in Eq. (1).

#243726 Received 25 Jun 2015; revised 14 Aug 2015; accepted 16 Aug 2015; published 15 Sep 2015

Appendix B: Serial calculation of discretized coupled mode equations

We apply the spatial discretization of *y*-infinite unit cells (Fig. 3(a)) and the causality condition for the potential momentum ($p,\ q \geq 0$) to the integral form of the coupled mode equations; thus, Eq. (2) becomes

$$\begin{aligned} &8\pi^2 i\cdot\left(\int_{S_R}\psi_{[k_x,k_y]}\cdot\frac{k_x}{\varepsilon_{y0}}dy-\int_{S_L}\psi_{[k_x,k_y]}\cdot\frac{k_x}{\varepsilon_{y0}}dy\right)\\ &=\int_V\iiint_0^\infty\left(\frac{(k_x-p)^2\Delta\varepsilon_{ypq}}{\varepsilon_{y0}^2}+\frac{(k_y-q)^2\Delta\varepsilon_{xpq}}{\varepsilon_{x0}^2}\right)\psi_{[k_x-p,k_y-q]}dpdqdv. \end{aligned} \tag{9}$$

We apply the subwavelength limit to evaluate the volume integral from the average of the values in S_L and S_R as

$$\begin{aligned} &\int_V\iiint_0^\infty\left(\frac{(k_x-p)^2\Delta\varepsilon_{ypq}}{\varepsilon_{y0}^2}+\frac{(k_y-q)^2\Delta\varepsilon_{xpq}}{\varepsilon_{x0}^2}\right)\psi_{[k_x-p,k_y-q]}dpdqdv\cong\frac{\Delta x}{2}\cdot\\ &\times\left(\int_{S_L}+\int_{S_R}\right)\iint_0^\infty\left(\frac{(k_x-p)^2\Delta\varepsilon_{ypq}}{\varepsilon_{y0}^2}+\frac{(k_y-q)^2\Delta\varepsilon_{xpq}}{\varepsilon_{x0}^2}\right)\psi_{[k_x-p,k_y-q]}dpdqdy \end{aligned} \tag{10}$$

For discretization in *k*-space with sufficiently small Δk (Fig. 3(b)), Eq. (9) can be approximated by the following equation for the m^{th} *k*-state:

$$\begin{aligned} &\int_{S_R}\psi_m(x_R,y)dy=\int_{S_L}\psi_m(x_L,y)dy\\ &+\sum_{n=1}^{m}\frac{\varepsilon_{y0}\Delta x\cdot\Delta p_n\Delta q_n}{16\pi^2 ik_{xm}}\cdot\left(\frac{{k_{xn}}^2\Delta\varepsilon_{ypq}}{\varepsilon_{y0}^2}+\frac{{k_{yn}}^2\Delta\varepsilon_{xpq}}{\varepsilon_{x0}^2}\right)\cdot\int_{S_L+S_R}\psi_n dy, \end{aligned} \tag{11}$$

where $p = k_{xm} - k_{xn}$, $q = k_{ym} - k_{yn}$, $\Delta p_n = k_{x(n+1)} - k_{xn}$, $\Delta q_n = k_{y(n+1)} - k_{yn}$, and *n* denotes each *k*-state before the m^{th} state. Because the spatial boundary condition is applied to the left side of the structure, the calculation is performed from the left to the right side in space. Additionally, because of the causality condition, *n* has the lower limit of $n = 1$, which is defined by the *k*-state of an incident wave (k_{x0},k_{y0}), and the calculation in *k*-space should be performed from $n = 1$ to $n = m$. Therefore, we separate the unknown and known integral terms in Eq. (11) as

$$\begin{aligned} &\left[1-\frac{\varepsilon_{y0}\Delta x\cdot\Delta p_m\Delta q_m}{16\pi^2 ik_{xm}}\cdot\left(\frac{{k_{xm}}^2\Delta\varepsilon_{y00}}{\varepsilon_{y0}^2}+\frac{{k_{ym}}^2\Delta\varepsilon_{x00}}{\varepsilon_{x0}^2}\right)\right]\cdot\int_{S_R}\psi_m(x_R,y)dy\\ &=\left[1+\frac{\varepsilon_{y0}\Delta x\cdot\Delta p_m\Delta q_m}{16\pi^2 ik_{xm}}\cdot\left(\frac{{k_{xm}}^2\Delta\varepsilon_{y00}}{\varepsilon_{y0}^2}+\frac{{k_{ym}}^2\Delta\varepsilon_{x00}}{\varepsilon_{x0}^2}\right)\right]\cdot\int_{S_L}\psi_m(x_L,y)dy.\\ &+\sum_{n=1}^{m-1}\frac{\varepsilon_{y0}\Delta x\cdot\Delta p_n\Delta q_n}{16\pi^2 ik_{xm}}\cdot\left(\frac{{k_{xn}}^2\Delta\varepsilon_{ypq}}{\varepsilon_{y0}^2}+\frac{{k_{yn}}^2\Delta\varepsilon_{xpq}}{\varepsilon_{x0}^2}\right)\cdot\int_{S_L+S_R}\psi_n dy \end{aligned} \tag{12}$$

We can now perform the serial calculation with the boundary condition $\int\psi_1(x{=}0)dy$. At the fixed point ($x = x_f$), all of the *k*-states can be obtained from Eq. (12) in the order $\int\psi_1(x{=}x_f)dy$, $\int\psi_2(x{=}x_f)dy$, …, $\int\psi_m(x{=}x_f)dy$. These results are applied to calculate the states at the next position ($x = x_f + \Delta x$). For a unity incidence wave on the boundary, the density of the envelope is directly proportional to the integral of the density of the envelope.

#243726 Received 25 Jun 2015; revised 14 Aug 2015; accepted 16 Aug 2015; published 15 Sep 2015

Acknowledgments

This work was supported by the National Research Foundation of Korea through the Global Frontier Program (GFP) NRF-2014M3A6B3063708, the Global Research Laboratory (GRL) Program K20815000003, and the Brain Korea 21 Plus Project in 2015, which are all funded by the Ministry of Science, ICT & Future Planning of the Korean government.

#243726 Received 25 Jun 2015; revised 14 Aug 2015; accepted 16 Aug 2015; published 15 Sep 2015